Bulletin of Engineering Geology and the Environment (2025) 84:317
https://doi.org/10.1007/s10064-025-04276-1

ORIGINAL PAPER

Swelling characteristics of red-bed mudstones from Southwest China at variable heat treatment conditions

Zhuowu Xie[1] · Xin Liao[1,2] · Inna Safonova[1] · Wei Wei[1] · Sixiang Ling[1,2] · Sergei Krivonogov[1,3] · Xiyong Wu[1,2]

Received: 16 April 2024 / Accepted: 23 April 2025 / Published online: 19 May 2025

Abstract

Mudstone swelling capacity is an important factor that determines the quality of engineering constructions, in particular, roads, tunnels, dams, etc. The most important parameter is the content of water that determines the stability/behavior of mudstone under different conditions, e.g., under variable temperature and humidity. Laboratory thermal treatment is a widely used method to measure the content of water in mudstone, which controls its swelling capacity. Exploring the swelling properties of samples treated at different temperatures will help to further understand the impact of water content on swelling properties. In this paper, we present new results on the heat treatment of red-bed mudstones of the Shaximiao Formation exposed in the eastern Sichuan Province of SW China in order to trace variations of mass, pore content, microstructural patterns and swelling characteristics. The swelling was traced by scanning electron microscopy and pore tester. The heat treatment changes the microstructure and pore characteristics of the mudstone and its swelling properties. The mudstones yielded three types of water loss patterns caused by the presence of free, absorbed and constitutional waters. The swelling properties appeared to depend on the pattern of the loss of three water types at different temperatures. The increasing temperature resulted in faster dehydration of clay minerals, stronger damage of original textures and microstructures (pore pattern) and stronger swelling. Our results provide a new guideline for selecting a temperature of heat treatment and controlling the content of water during red-bed swelling experiments.

Keywords Red-bed mudstone · Drying temperature · Microstructure · Pore characteristics · Swelling characteristics

✉ Xin Liao
xinliao@swjtu.edu.cn

Zhuowu Xie
xie9204@126.com

Inna Safonova
inna03-64@mail.ru

Wei Wei
lamborww0801@sina.com

Sixiang Ling
lingsx@swjtu.edu.cn

Sergei Krivonogov
s_krivonogov@mail.ru

Xiyong Wu
wuxiyong@swjtu.edu.cn

[1] Faculty of Geosciences and Engineering, Southwest Jiaotong University, Chengdu, Sichuan Province 611756, PR China

[2] Sichuan Province Engineering Technology Research Center of Ecological Mitigation of Geohazards in Tibet Plateau Transportation Corridors, Chengdu 611756, China

[3] Korkyt Ata Kyzylorda University, Kyzylorda 120014, Kazakhstan

Introduction

Mudstone is a sedimentary clastic rock dominated by clay minerals. Mudstones are widely distributed in warm and dry to humid areas, like central and southwest (SW) China (Fig. 1a), where they often form so-called red beds. The extensive construction in that region with abundant red beds meets problems with fluctuating water contents in surficial and deep mudstone layers due to both natural and artificial (man-induced) processes. The natural variations of the water content in water-sensitive rocks like mudstones depend on climate-related factors, such as rainfall, groundwater level and surface runoff. Such rocks are greatly affected by seasonal changes of the volume of groundwater and thermal-hydraulic cycles in the areas with warm climate and by the freeze-thaw cycles in cold areas (Doostmohammadi et al. 2009; Lu and Wang 2017; Lu et al. 2021). Therefore, the study of mechanisms of water-rock interactions, e.g., moisturizing and swelling, that may induce disintegration and shrinkage of mudstone, are of high importance.

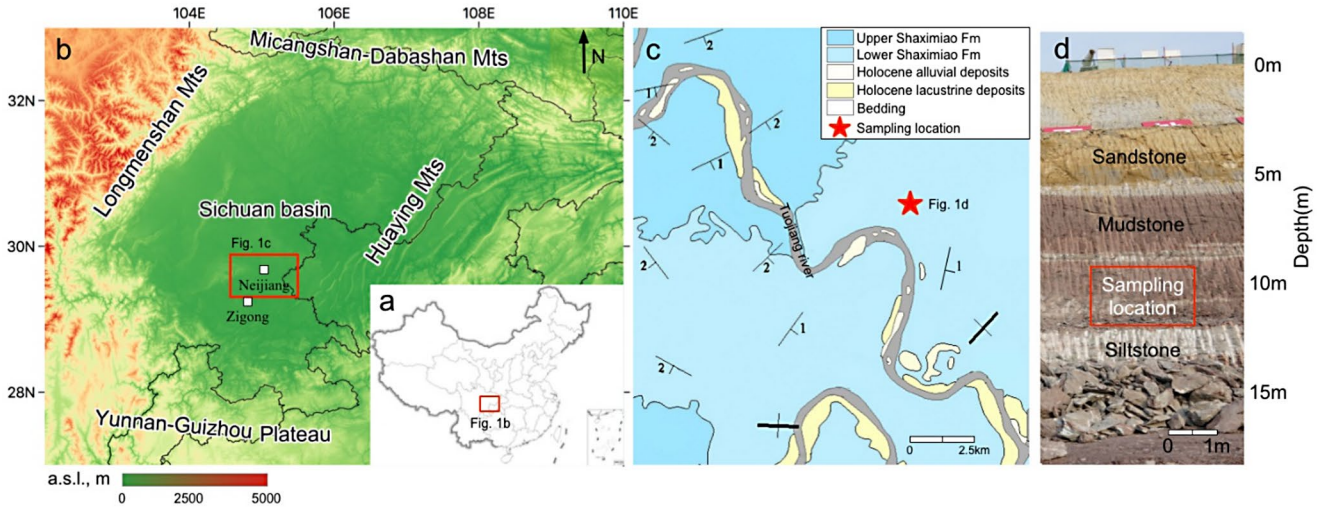

Fig. 1 Overview of the study area. **a** - geographic position; **b** - topography of the Sichuan Basin (a.s.l., m – metres above sea level); **c** - geology of the sampling area and the sampling sites; **d** - outcrop of the Shaximiao Formation

Rock swelling is an important factor affecting the safety of geotechnical engineering, for example, the post-construction bulge deformation of the foundation of high-speed railway ballast track that must be less than 4 mm (Dai et al. 2021). Therefore, to obtain accurately values of rock swelling rates during indoor testing is crucial. In rock mechanics, the swelling properties of red-beds have been traditionally studied by using drying-wetting experiments (Okamoto et al. 1981; Pejon and Zuquette 2002; Zhang et al. 2010). Such experiments require a sample to be dried before the experimental run to obtain maximum swelling rates. Heat treatment is commonly used to prepare completely dried samples, and therefore a key problem is to select an appropriate drying temperature. Previous studies have focused on the mechanical properties of rocks at the room temperature and up to 200 °C and revealed different effects of the temperature on rock strengthening or weakening (Wu et al. 2006; Yavuz et al. 2010; Yang et al. 2017a, b; Yin et al. 2016). The results from different research groups appeared contradictive though. Several researchers have reported that the rocks get stronger at an increasing temperature (Chen et al. 2012; Singh et al. 2015). The others mention that the changes of the temperature have no effect on the strength of the rocks (Yin et al. 2016; Zhang et al. 2016a, b; Gautam et al. 2018). In addition, there have been obtained data showing that the temperature has a weakening effect (Ferrero and Marini 2001; Kumari et al. 2017; Gautam et al. 2018; Sirdesai et al. 2017, 2018).

Another important issue is the evaporation of water near the boiling point and above. Such a process has not been studied well, in particular, in terms of rock swelling properties (Wong et al. 2020). As we know, the swelling of sedimentary rocks depends on the initial content of water, the rate of mineral expansion, and the microstructure (Liu et al. 2021a, b; Taylor and Smith 1986; Zhang et al. 2010). The heat treatment is one of the most critical factors of swelling that changes the initial water content. The mineral composition of the rock is stable below 200 °C, but the consolidation properties of clay minerals start to change at 90 °C (Towhata et al. 1993) resulting in decreased rock strength. The heat-sensitive minerals, e.g., calcium sulfate dehydrate ($CaSO_4$-$2H_2O$), malachite ($Cu_2(OH)_2CO_3$) and clay minerals (montmorillonite-chlorite-illite), can be transformed only at 200 °C and higher (Tian et al. 2012). In turn, a change of rock microstructure significantly influences on rock permeability (Tian et al. 2014) and related swelling properties (Liu and Xu 2014). Therefore, the experiments performed at different heat treatment temperatures may change the content of water, the swelling properties of rocks in general and the swelling patterns in particular.

Study of the swelling properties of red-beds is of special importance for the construction of high-speed railways, because the expansion characteristics of roadbed material determine the smoothness of the railway track. In SW China, the high-speed railways are erected on roadbed materials or rocks capable to expand, i.e., red-beds. In contrast to many other red-bed formations, the red beds in SW China are characterized by significant swelling and shrinking during wet and dry seasons, respectively. Previously, it has been found that in spite of a required series of pre-construction tests made for soft expansive rocks (like red-beds) in the study area, the bedrocks started to uplift (Dai et al. 2021; Huang et al. 2023). Two reasons were proposed: in-situ tectonic stress on the steeply dipping mudstone strata, and misleading heat treatment pre-assessment of swelling. We propose that the existing standards including also experiments on the

heating (PRC National Standard 2013) cannot reliably evaluate potential swelling of red-beds. Accordingly, we carried out several heat treatment experiments under varying temperatures to evaluate the influence of different temperatures on the fracturing and swelling accuracy as a function of mudstone hydration and changes of microstructures and pore patterns.

Geological setting and sample preparation

The Sichuan Basin is bounded by the Wushan, Longmenshan, and Dabashan orogenic belts in the east, west, and north, respectively, and by the Yunnan–Guizhou Plateau in the south (Fig. 1a, b). Topographically, the Sichuan Basin is a hilly. Geologically, the basin consists of Precambrian basement and Palaeozoic marine deposits that are overlapped by Mesozoic terrestrial strata (Bureau 1980). The Mesozoic deposits are mainly Jurassic and Cretaceous in age, with a subordinate number of Triassic sedimentary rocks of onshore origin. The study area is dominated by sedimentary rocks of the upper Shaximiao Formation (J_{2s^1}) and lower Shaximiao Formation (J_{2S^2}), late Pleistocene alluvial deposits (Q_3^{al}), and Holocene lacustrine and alluvial deposits (Q_4^{l+2al} and Q_4^{3al}, respectively). The mudstone samples come from the upper Jurassic Shaximiao Formation (Fig. 1c), whose deposits are widely distributed around the cities of Neijiang and Zigong in the eastern Sichuan Basin. The formation is dominated by purple and red mudstones plus siltstone and sandstone composing horizontally or gently inclined strata.

The purple, brick and red mudstones were sampled from a 10 m-deep quarry (Fig. 1d) near a tunnel north of the Neijiang North Station in Sichuan Basin. The stratigraphy and lithology of these rocks are almost identical to those that form the foundation of the railway line of the Neijiang North Station. The rocks are poorly cemented and easily disintegrate, resulting in tiny cracks on the surface. Three samples collected for mineral analysis were obtained from a single one-metre-in-diameter piece of rock. The samples consisted (in average volume percent) of quartz (39.9%), feldspar (5.6%), plagioclase (20.2%), calcite (5.9%), haematite (2.1%), mica (1.6%), and clay minerals (24.7%). The clay minerals (taken as 100%) were illite (21%), kaolinite (4.04%), chlorite (4.04%) and a 1:1 mixture of illite and montmorillonite (70.92%). We prepared 75 short cylinders of mudstones that were 50 mm in diameter and 20 mm thick (± 1 mm) by air-cooled drilling.

Table 1 Experimental groups and parameters

Set	Sample number	Temperature ranges, °C	Temperature group
N-1 ~ N-35	1 ~ 5, 6 ~ 10	50, 70	LT
	11 ~ 15, 16 ~ 20, 21 ~ 25	90, 100, 110	MT
	26 ~ 30, 31 ~ 35	130, 150	HT
P-1 ~ P-35	36 ~ 40, 41 ~ 45	50, 70	LT
	46 ~ 50, 51 ~ 55, 56 ~ 60	90, 100, 110	MT
	61 ~ 65, 66 ~ 70	130, 150	HT
Y-1 ~ Y-5	71 ~ 75	25	CG

Testing groups: LT, low-temperature; MT, medium-temperature; HT, high-temperature; CG, control

Methodology of experiments

Experimental flow chart

The 75 samples were divided into three sets: set N for heat treatment testing, set P for swelling characteristic analysis, and set Y as a control group (CG, Table 1). Five samples were used for replicate tests at every temperature level. The temperature were divided into four groups: control (25 °C, CG), low-temperature (50–70 °C, LT), medium-temperature (90–110 °C, MT) and high-temperature (130–150 °C, HT) groups. Each sample was first dried at 50, 70, 90, 100, 110, 130, and 150 °C and then investigated. The experimental run consisted of five steps: (1) heat treatment, (2) a Brazilian test, (3) scanning microscopy observations, (4) N_2 absorption and desorption tests, and (5) a swelling rate experiment.

Heat treatment and temperature selection

Thermogravimetric analysis (TGA) clearly reveals compositional changes in the clay-rich minerals of mudstone caused by high temperatures (Zhang et al. 2016a, b; Yang et al. 2017a). Montmorillonite and illite typically yield three changes in the TGA curves at temperatures of 126, 650 and 906 °C. The overall mineral composition of mudstone changes at 650 and 906 °C. Accordingly, we chose seven heat treatment temperatures, i.e., 50, 70, 90, 100, and 110 °C, which did not change the mineral composition, and 130 and 150 °C that would change adsorbed water. Considering the discrete properties of natural rock samples, the mass versus time curve of the heat treatment were plotted using the "relative drying mass" formula:

$$\mathrm{RDM} = 1 - \frac{m_{iavg}}{m_{150avg}} \times 100\% \quad (1)$$

where m_{iavg} is the average drying mass loss of each group (i = 50, 70, 90, 100, 110, 130, 150) and m_{150avg} is the average value of mass loss at 150 °C.

Swelling experiment

According to the experimental flow chart (Sect. 3.1), the rock samples were placed in a desiccator and cooled at room temperature. After the cooling, we put vaseline onto the sides of each sample to minimize friction. The samples were placed individually in the device used for measuring swelling and soaked with water. Swelling was measured with a micrometer by increasing the sample thickness every 600 s. The experiment was stopped when the thickness stopped to increase. Each experimental run lasted 60 h. Five parallel test samples were used for each temperature group at different temperatures.

The swelling rate was calculated by the following formula:

$$\varepsilon = \frac{\Delta H}{H_0} \tag{2}$$

where H_0 is the thickness of the sample before the test, and ΔH is the change in the thickness of the sample during the experiment.

Microstructure and porosimetry

The microstructures of the samples were studied using a ZEISS EVO10 scanning electron microscopy (SEM) instrument equipped with a Leica EM ACE 200 28 nm golden ion sputter (sample pretreatment), a JSM-IT 500 tungsten lamp, and an OXFORD X-Max 80 energy dispersive spectrometer (EDS). To exclude the influence of tensile strength on the samples, we studied the microstructures on the freshly cracked surfaces that appeared after the Brazilian test. An ion sputter was used to create a conductive layer on the poorly conductive rock samples.

For the pore tests, we used an accelerated surface area and porosity system (ASAP2460). The samples were treated at different temperatures and then broken into pieces using sharp instruments to avoid pore crushing. Both the heat-treated samples and the initial samples were tested for pore size after 4 h under a vacuum in an ASAP2460 machine. For pore classification, we used theInternational Union of Pure and Applied Chemistry method (Thommes et al. 2015). The curve lacking a clear saturated adsorption platform implies an extremely irregular structure, including flat slit structures, cracks, and wedge outs. The hysteresis loop generated by the pore geometry induced by capillary condensation illustrates the irreversibility of the adsorption and desorption processes. The separation of the adsorption and desorption branches within the hysteresis loop is attributed to the level of liquid fixed during the alternating episodes of condensation and evaporation. Note that to obtain correct results on the distribution of pore sizes, we use the data on adsorption or desorption separately.

Results

Water loss during heat treatment

With increasing heat treatment temperature, the saturated vapour pressure in the dry oven increases and the relative air saturation decreases. The water gradually evaporates from the samples, ultimately reaching a dynamic phase equilibrium. Figure 2 shows the mass losses of the samples after LT, MT, and HT heat treatments, with the maximum, minimum and average values of five tests per sample. The time versus relative drying mass curves for each group of the samples show two different stages of dehydration, as shown by the two segments of the curves, i.e., convex and linear, which represent rapid and slow dehydration, respectively.

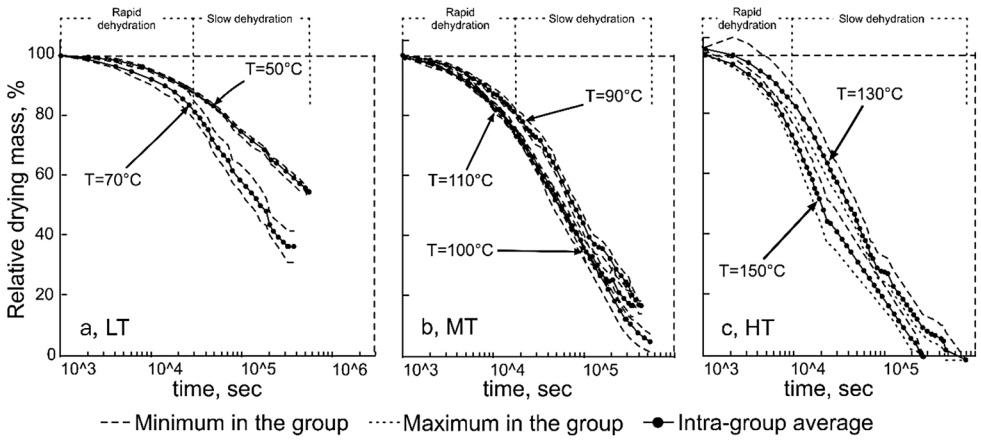

Fig. 2 Relative drying mass versus time curves at different heat treatment temperatures; **a** – low-temperature (LT group); **b** – medium-temperature (MT group); **c** – high-temperature (HT group)

The three groups exhibit rapid dehydration trends in the beginning, followed by stages of slow dehydration. The rapid dehydration phase is shorter in the HT group than in the LT group. When the temperature is less than 130 °C, the water loss of the sample is positively correlated with the temperature. The total amount of water lost in the HT group is the same. The first stage involves the rapid evaporation of free water. The second stage includes the slow transformation of absorbed or weakly bound water to free water and its evaporation.

Swelling after heat treatment at different temperatures

Figure 3 shows the swelling rates of the samples after heat treatment of different temperatures. The expansion in all heat treatment temperature groups lasts for approximately 50,000 s, and then the process stops. The samples pass rapid, slow, and plateau phases and their swelling rate clearly changed at 25,000 and 50,000 s. In the rapid growth phase, the rate of swelling of the HT group samples appeared much higher than that of the other groups; the maximum swelling rate is fixed at 130ºC and 150ºC. The swelling rate decreases with decreasing sample heat treatment temperature. In the HT group, the swelling rate is 1.11-1.05-1.17 times greater than that in the MT group, 1.22–1.16 times greater than that in the LT group, and 1.45 times greater than that in the CG group. Therefore, the temperature of heat treatment can significantly affect the rate of swelling.

As shown in Fig. 3b, the standard deviation within each group is clearly different at different temperatures. At the end of the rapid phase (t=25000 s), the intragroup discreteness of the swelling rate is the greatst in the HT group. At the end of the slow phase (t=50000 s), the intragroup standard deviation decreases in the MT and LT groups. At the end of the plateau phase (t=200000 s), the deviation is minimal in the HT group.

Figure 4 shows the swelling rate and absolute mass loss for each experimental group at different heat treatment temperatures. The swelling rates of the samples range from 28.01% (~25 °C) to 39.05% (~150 °C), and the absolute mass loss values range from 1.94 to 4.26 g. The heat treatment temperature is positively correlated with the swelling rate and degree of dryness of the samples. Notably, the rates of swelling and absolute mass loss are abnormal in the MT group. In addition, the swelling rate at 100 °C displays a significant intragroup dispersion. The swelling rate and absolute water losses at 130 °C and 150 °C are similar.

Microstructural features after heat treatment

After the heat treatment, the clay minerals get parallel orientation to form typical planar, sheet, and layered structures (Fig. 5). There are two types of microscopic layer structures: (1) interlayer fractures with grain shedding, i.e., the LT and MT groups (Fig. 5a-e); and (2) dominant interlayer fractures and subordinate interlayer fractures, i.e., the HT group (Fig. 5f-h). The 0.5–2 nm mud particles are typical of all

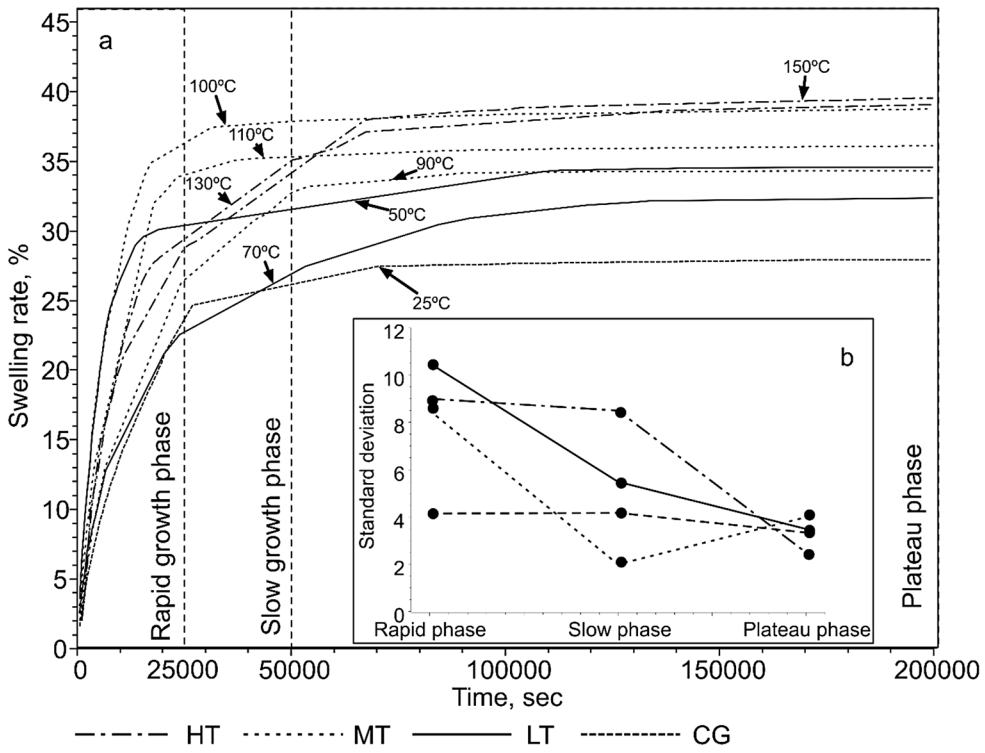

Fig. 3 Temporal characteristics of swelling. **a -** swelling rate curve; **b -** standard deviation within each group during t=25,000, 50,000 and 200,000 s. Abbreviations refer to Table 1

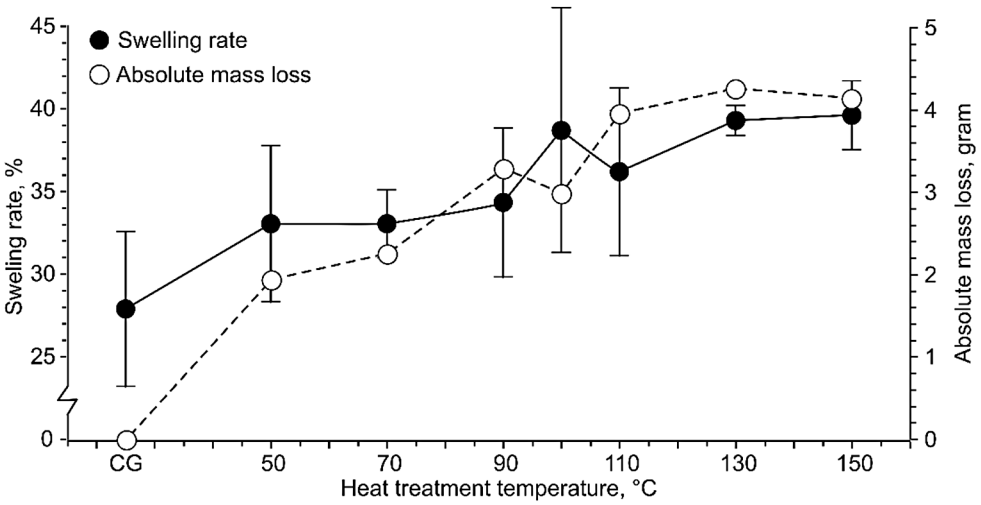

Fig. 4 Swelling rate and mass loss characteristics versus heat treatment temperature

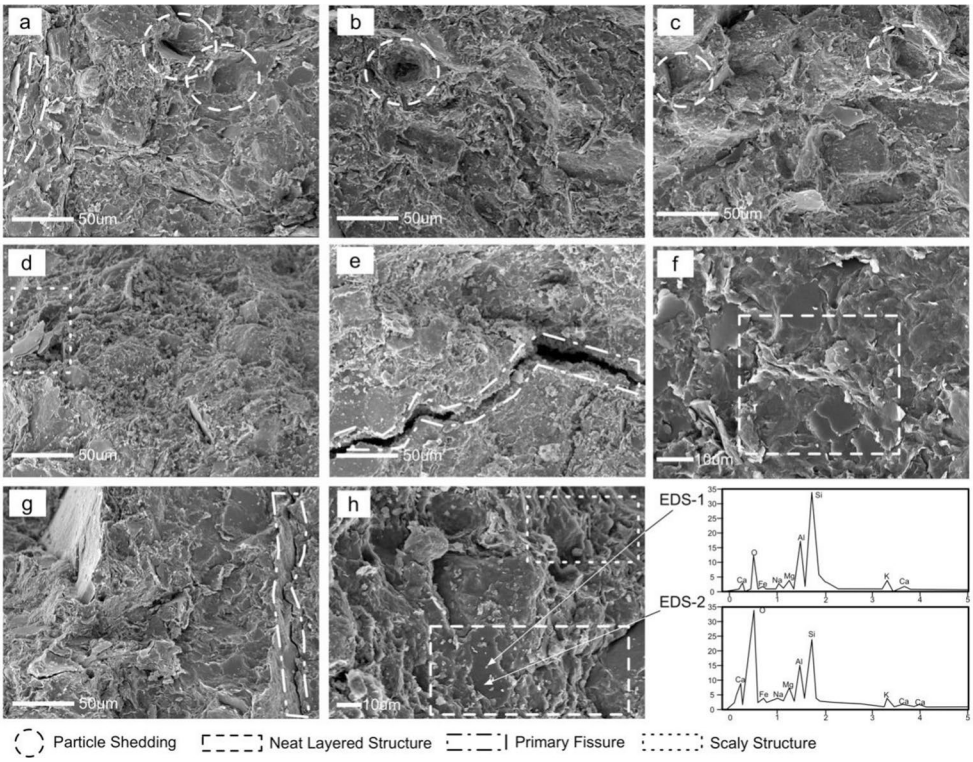

Fig. 5 Microstructures at different heat treatment temperatures. SEM-images at 500X. **a**-**b** - LT group, samples N-4, N-8; **c**-**e** - MT group, samples N-17, N-23; f-h - HT group, samples N-26, N-32, N-35; EDS-1 for the particles in SEM images; EDS-2 for the lamellae in SEM images

groups, but the portion of those particles is larger in the LT group (Fig. 5a, b). The LT heat treatment ultimately caused shedding of mineral particles (Fig. 5a-c). The results of the multipoint EDS test show that the particles represent plagioclase agglomerations. This suggests that the evaporation of water from rock samples during heat treatment causes mineral exfoliation, and the exfoliated particles are concentrated in pores and fractures. The heated samples acquire microscopic fissures significantly different from those of the original rock samples. The variances observed in the SEM images of the three groups indicates that the heat treatment changed the microstructure of the mudstone samples after the heat treatment.

Microscopic pore features

Figure 6 shows the results of micropore volume determination in each temperature group via nitrogen absorption/desorption method. The cumulative pore volume and pore area after the heat treatment range from 16.259 ~ 14.601 mm^3/g and 18.320 ~ 15.911 m^2/g, respectively. The values for the control group are 9.126 mm^3/g and 7.061 m^2/g, respectively. The volume and area ratios relative to those of

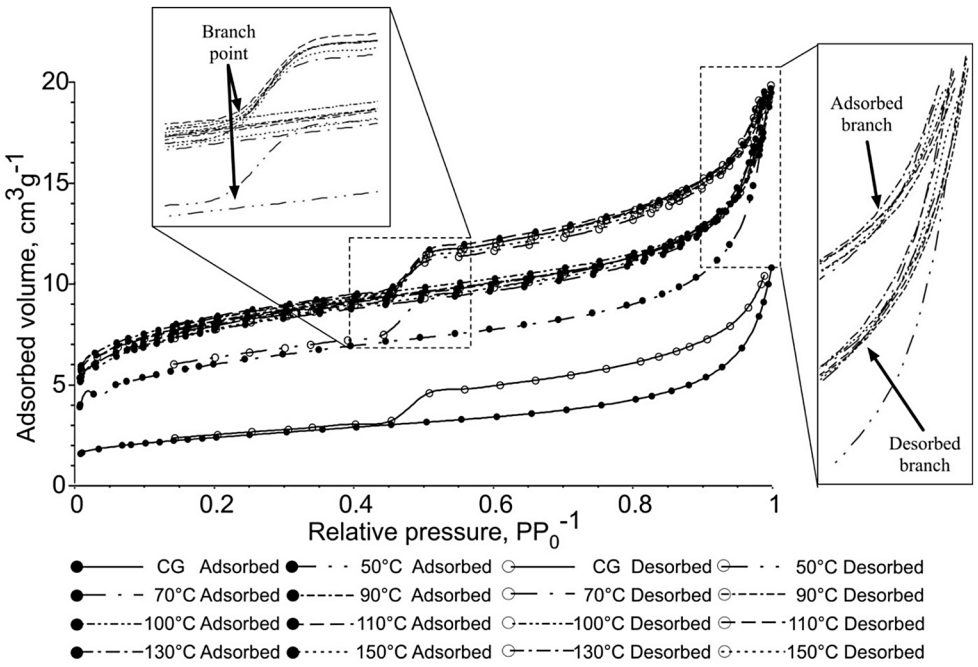

Fig. 6 Low-pressure N_2 adsorption and desorption isotherms

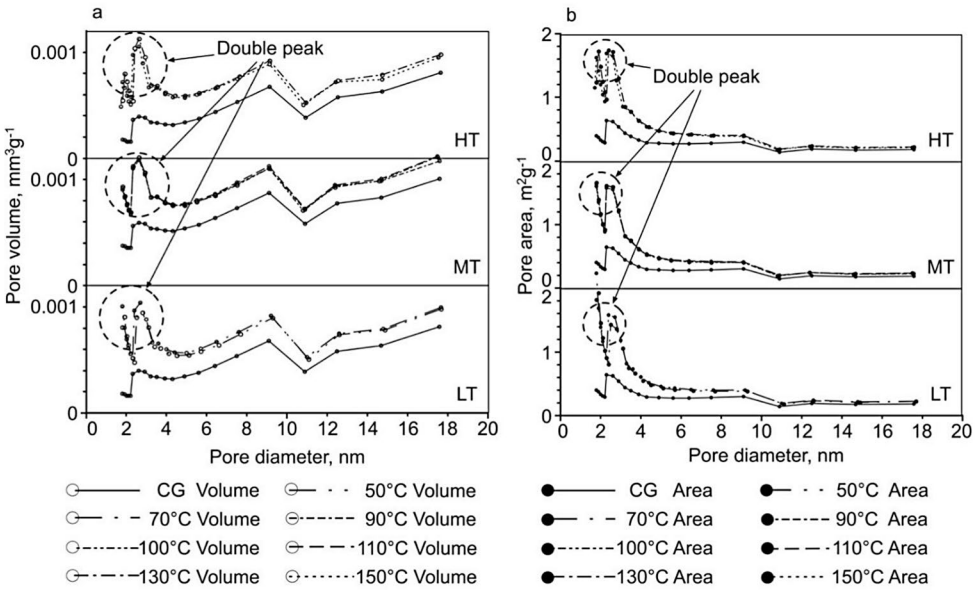

Fig. 7 Pore volume (**a**) and pore area (**b**) related to the pore diameter in different temperature groups during absorption. The abbreviations in the legend are listed in Fig. 6; Table 1

the control group are 1.949 and 2.561 (HT /CG), 1.815 and 2.280 (MT /CG), and 1.981 and 2.593 (LT /CG), respectively. Different adsorption and desorption curves after the branch point indicate various types of pores. The absorption/desorption curves suggest that the samples carry H3-type pores, which are layered structure according to the International Union of Pure and Applied Chemistry (IUPAC) classification (Thommes et al. 2015).

Figures 7 and 8 illustrate the relationships between the pore diameter, volume, and area as a function of the temperature of adsorption and desorption. The results show that the pores are mostly 2–5 nm in diameter plus a smaller peak at 0–2 nm. The impact of the heat treatment on the relative number of pores larger than 7 nm is minimal. The pore size–volume distribution curve shows a similar overlap, but the curves for pore less than 5 nm in diameter are different. The adsorption and desorption curves of the LT group is significantly vary with temperature, and the distribution curves of the pore diameter are different for the 0–10 nm interval. During heat treatment, the overall quantity of pores increases. Both the incremental pore area and volume also significantly increase, indicating the appearance of micropores as a result of the release of the interlayer water and the presence of clay. The appearance of such mineral-scale pores changes the overall pore structure.

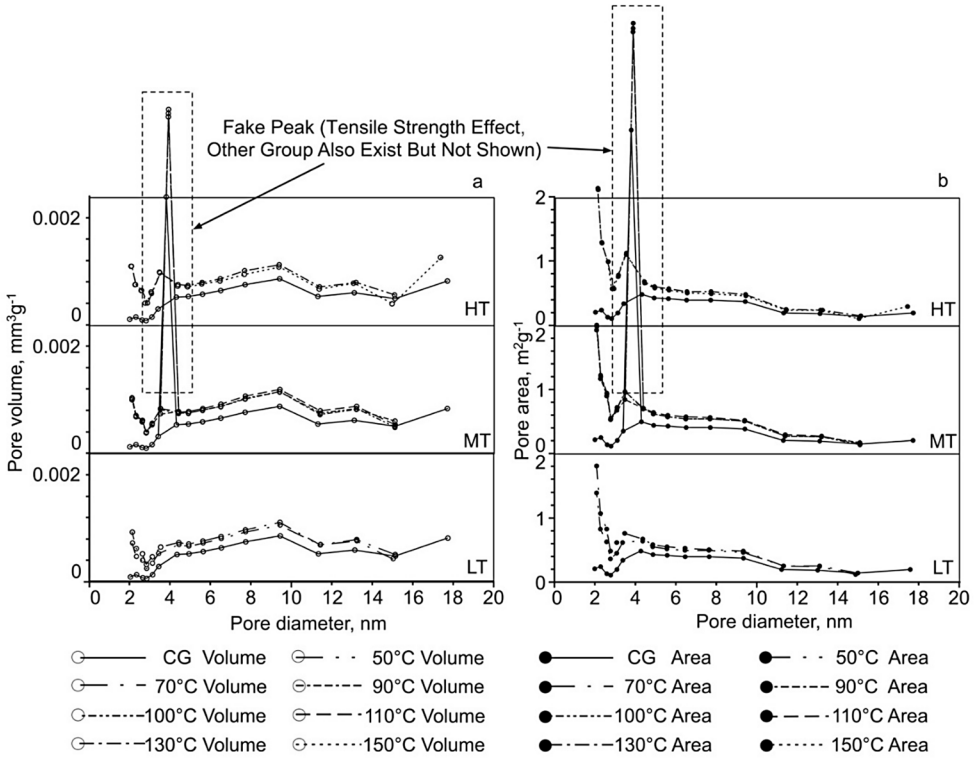

Fig. 8 Pore volume (**a**) and pore area (**b**) related to the pore diameter in different temperature groups during desorption. The abbreviations in the legend are listed in Fig. 6; Table 1

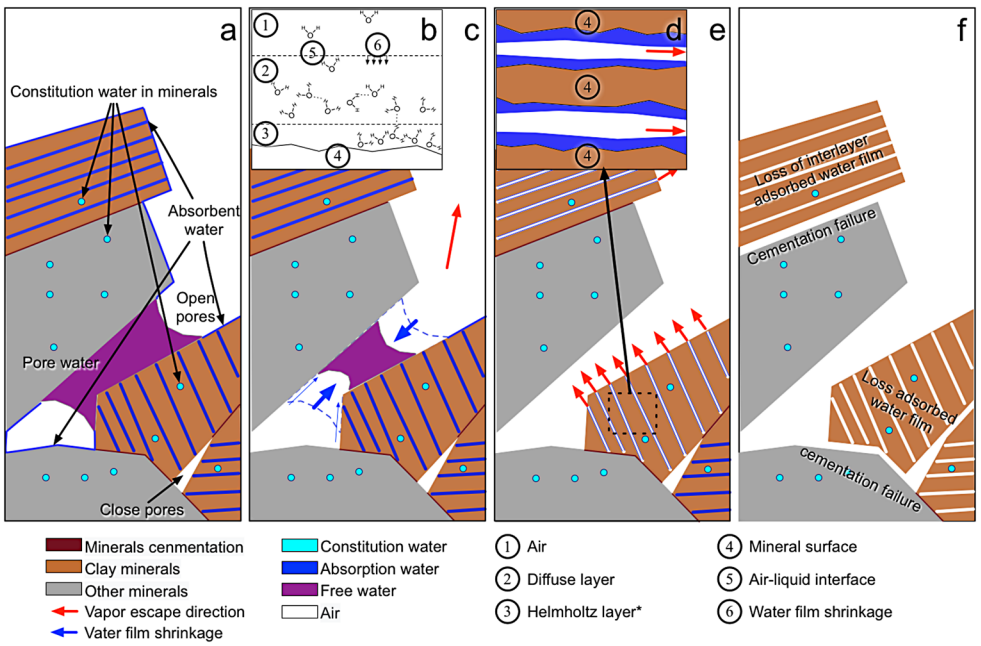

Fig. 9 Mechanisms of water loss in different temperature groups. a - natural state of the mudstone samples from the Shaximiao Formation; b - water at the mudstone surface (Karaborni et al. 1996; Fernandes et al. 2019); c - LT heat treatment; d - interlayer water in clay minerals. e - MT heat treatment; f - HT heat treatment

Discussion

Water loss at different heat treatment temperatures

Previous scholars have recognized three types of water in mudstones on the basis of the strength of water molecules bound to minerals (Fig. 9a): (1) free water present in large pores and fissures connected by hydrogen bonds; (2) water adsorbed on mineral surfaces and Helmholtz surfaces, also called interlayer water associated with layered clay minerals (Zhang et al. 2024; Cliff 2018); and (3) constitutional water present in a mineral lattice and therefore representing an essential component of the mineral structure (Fernandes et al. 2019; Li et al. 2019). There is still no agreement on how to determine the degree of evaporation during actual water evaporation. In general, the heat treatment temperature

determines which forms of water the rock sample loses. At a macro level, external thermal energy causes water to migrate as vapour or liquid and then to spread over a gas–solid/liquid–solid interface. At a micro level, external heat promotes Brownian motion (Lahn et al. 2019) and breaks the van der Waals forces between water molecules or water and mineral molecules.

During heat treatment, water in rocks typically migrates as a liquid under the influence of surface tension or gas (liquid–gas phase transition). Water is first removed from the outer parts of the sample, as the hydrogen bond energy between water molecules is much less than that between water–mineral compounds (Bond and Willis 1969; Miller et al. 1991). At the beginning of heat treatment, free water releases first. As the temperature increases, the adsorbed water get released to bind the water on the surface of hydrophilic minerals. Further increase of the temperature destroys hydroxyl components in mineral crystal lattice.

Figure 9 illustrates mechanisms of water loss from red-bed mudstone at different temperature conditions. The released water may either change from liquid to gas and then slowly dissipate or it may evaporate rapidly to dissipate on the gas-liquid interface. If the temperature rises rapidly, as in the case of the HT and MT groups, the water will first change to gas phase and then the water molecules dissipate. The heat treatment at a temperature significantly above the boiling point of water leads to the reduction of cohesion between water molecules and its direct evaporation. This process induces microstructural changes and affects the size and volume of the pores. If the temperature increases slowly, as in the case of the LT group, the external energy would facilitate the Brownian motion and the removal of water molecules from the sample through cracks and pores (Fig. 9d, e), and reduce the area and thickness of the pore water film (Figs. 9b, c, respectively). Therefore, the rate of dehydration determines the structure of the pores after the heat treatment (Fig. 9f).

Microstructure and porosity changes

Porosity is an important factor influencing the physical and mechanical properties of rocks. High-temperature conditions generally promote an increase in the number and size of pores (Jin et al. 2020). Shen et al. (2023) conducted heat treatment experiments on coal-bearing mudstone at different temperature; the results indicate that the pore volume is negatively correlated at temperatures less than 200 °C, but positively correlated at temperatures ranging from 200 to 800 °C. Zhang et al. (2017) reported no significant changes in the pore structure of sandstones at 200 °C, in which the pore size increased sharply from 200 to 500 °C. Xu et al. (2010) reported that temperatures of 800 °C and 1200 °C are critical for changes in the pore structure. According to our experiments, high temperature affects porosity in two ways. In one way, the expansion coefficient of the rock increases and the porosity decreases. In another way, the high temperature increases the evaporation of water from the interior of the rock, which in turn increases the porosity. Therefore, the two ways could either reduce or increase the swelling, respectively.

The number, size and distribution patterns of pores may change under different heat treatments (Towhata et al. 1993). In our experiments with the HT samples, the water freely dissipated as gas from the open pores; in the closed pores, the heating expanded the gas and increased the pressure (Fig. 9e, f) to trigger the formation of microcracks. In thermodynamics, water evaporation depends on the temperature, absolute ambient humidity and heat treatment time. The "bimodal" distribution of micropores under different heat treatment regimes can be partly explained by the loss of interlayer water due to the extended heat treatment time. During the LT heat treatment, the water slowly migrates through the water-gas boundary. The outside thermal energy does not completely remove the water from the samples, which remains in all types of pores.

Figure 10 shows the trends of changes in the pore volume and area with increasing temperature. The absence of clear correlation between the pore area and pore volume suggests different types of pores in the samples. The pore area, pore volume and swelling rates all show significant abnormal fluctuations at approximately 100 °C (Fig. 10). Such phenomena can be explained by the different effects of evaporated water on the microstructure of the samples during heat treatment at different temperatures.

The SEM images (Fig. 5) show that the HT heat treatment causes the formation of macrofractures and laminated structures in the minerals due to expansion. Therefore, the HT treatment disrupts the integrity, weakens the interlayer structure and induces interlaminar fracturing. In the MT group, the fine particles attached to the layered structure of the clay minerals, appear at a temperature close to the boiling point of water. Therefore, we can conclude that the homologous compounds of the clay minerals in the MT group produce microstructural features completely different from those of the HT and LT groups. The rate of water evaporation in the MT group is lower than that in the HT group, suggesting that mainly free water was evaporates during the early phase. During the late phase, the weakly bound water evaporates incompletely: first it transforms into free water and then evaporates. This process is consistent with the clear inflection point in the curve showing the MT group. Moreover, the layered structure observed on the clay minerals in the SEM images, indicates that the HT heat

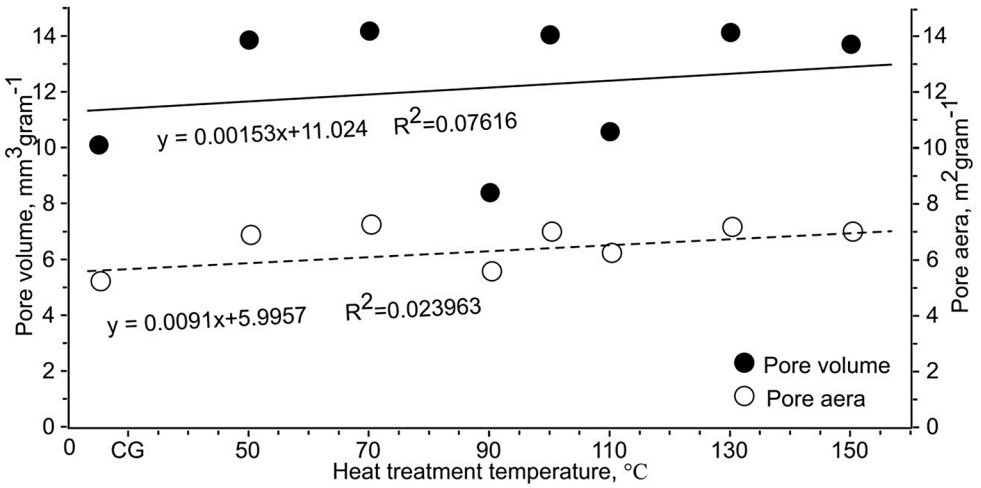

Fig. 10 Pore volume and pore area at different heat treatment temperatures

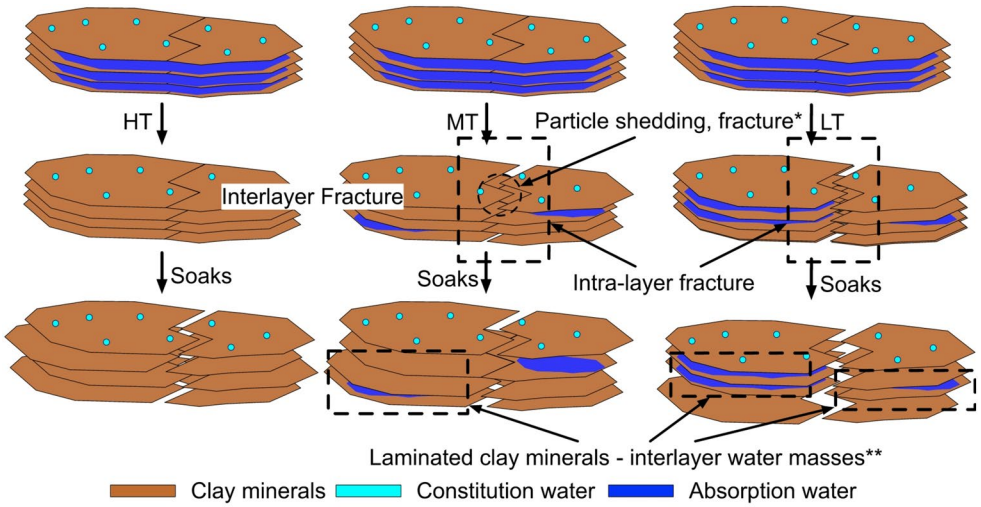

Fig. 11 Mechanisms of swelling for the HT, MT and LT groups. The primary cutting fractures may cause fragmentation and dislodgement of fine-grained clay minerals as shown in the SEM images. The hydrogen bonds between water molecules are weaker than those between cations and water molecules, and the laminated clay minerals, which are not completely stripped from the interlayer water, form specific structures of "laminated clay minerals - interlayer water masses" structures, that limit the swelling

treatment removes the water that originally fills microcracks and pores.

Mechanisms of swelling

Clay minerals play a significant role in the swelling of red-bed mudstones. Swelling depends on the presence of clay particles less than 0.002 mm in size, which have free valence atoms and ions on their surface (Liu et al. 1999). The electrostatic gravitational force of clay particles can create an electrostatic gravitational field on their surfaces, which causes special intermolecular interaction forces between hydrogen atoms and electronegative oxygen atoms or cations leading to covalent bonding (Mitchell 1993; Laird 2006). These bonds amplify the adsorption force of the clay particles, which can reduce the molecular mobility of water. The swelling of clay minerals implies surface hydration and osmotic hydration (Huang et al. 2023). Water first seeps into large pore structures and then into the lamellar structures of the absorbent minerals. Moreover, the water adsorption process changes the pore area and volume (Li et al. 2019, 2021; Barshad 1952).

In general, the presence of cations, the type of homocrystalline substitution and the state of microstructural stacking determine the swelling behavior (Saiyouri et al. 2000; Hueckel 1992). The cation exchange capacity is an important indicator for assessing the expansion potential of clay minerals. It can increase during heat treatment because of the formation of more fissures and pores. The evolution of the microstructure of red-bed mudstone greatly influences its swelling. Therefore, an inappropriate selection of heat treatment temperatures would ultimately result in an inaccurate measurement of the swelling rate.

Figure 11 shows the mechanism of swelling of red-bed mudstone after heat treatment at different temperatures (HT, MT, and LT). The HT group shows removal of almost all the water from the samples. A small amount of adsorbed water is retained between the clay mineral layers in the MT group, and the LT group contains even more adsorbed water.

The heat treatment resulted in the formation of intra-layer and inter-layer fractures according to SEM images (Fig. 5). This indicates that temperature affects the state of microstructure stacking in the mudstone, that is consistent with previous studies (Delage et al. 2006; Pusch et al. 1990). The results of porosimetry reveal changes in the pore structure during dehydration. The transformation of free and adsorbed water into a gaseous state changes the structure of the pores (Wong et al. 2020). The bimodality of the 0.5–2 nm pores (Figs. 7 and 8) may indicate a loss of adsorbed water in the stratified structures of the samples. The mass loss curves (Fig. 2) and changes in the pores and microstructures at different heat treatment temperatures suggest a close relationship between swelling of rock samples and water loss. Our results show that the swelling rate is strongly correlated with temperature, but poorly correlated with the pore area and volume. Changes in the microstructure of the expansible clay minerals at various temperatures result in different swelling processes. Water penetrates into cracks and micropores first. Expansible minerals may undergo deformation, displacement and fragmentation leading to the acceleration of swelling (Van Geet et al. 2005). After such an initial swelling, the air in the pores would prevent water further penetration, and the layered structure of clay minerals, if it is not completely dehydrated, will restrain swelling. Our results (Figs. 4, 5 and 9a) show that free water and partially absorbed water allow the expanding minerals to retain a part of their original structure at lower heat treatment temperatures. However, the original layered structure of the sample would get destroyed if the temperature of treatment exceeds 130 °C. In addition, the dispersion of the swelling results of the HT group is significantly lower than that in the other groups (Fig. 4). The impact of the discreteness of rock samples on the swelling rate can be efficiently reduced at appropriately higher temperature of heat treatment.

Conclusions

In our study, different scenarios of drying and swelling were investigated to evaluate the effect of heating temperatures on the microstructure and pore structure of mudstones of the Shaximiao Formation in the eastern Sichuan Basin. Heat treatment significantly changed the number of pores and the microstructural characteristics of the mudstone. The temperature of heat treatment is positively correlated with the number and volume of pores. The pore distribution plots shift from “single peak” to “double peak” as the size of the pores changed from 0.5 to 2 nm. The heat treatment at 150 °C and 130 °C disrupted the pre-existing clay mineral-water-clay mineral layered structure, whereas that at 110 °C to 50 °C resulted in the generation of a higher number of micro-fragments.

The pore area versus pore volume of the heat-treated samples shows a positive correlation with the swelling rate, but both showed anomalous fluctuations around the boiling point of pure water at the atmospheric pressure. The heat treatment temperature is positively correlated with the amount of mass-loss and the rate of swelling of the heat-treated samples. These two correlations are not linear or exponential though. The heat treatment can also reduce the effect of various individual properties of rock samples on the swelling test.

The environment-related (humidity, air temperature) can change the properties of the fluvio-lacustrine sediments of the Shaximiao Fm. and lead to the formation of different structures of mudstone layers. The heat treatment at low temperatures cannot fully remove water out of a rock sample. The water release patterns can be effectively changed by selecting different regimes/temperatures of heat treatment. Therefore, the temperature of heat treatment must be slightly lower than the temperature of the thermal stability of the sample under drying. The mudstones of the Shaximiao Fm. should be dried at a temperature higher than 130 °C, as it can give reliable swelling measurement results without composition changes.

Acknowledgements This research is funded by the National Natural Science Foundation of China (No. 41877215, XYW, No. 42477200, XL), Chengdu Science and Technology Program (2022-YF05-00340-SN, SXL), Fundamental Research Funds for the Central Universities of China (2682023CX016, IS), Key R&D Program of Sichuan (Project #2022YFWZ0009, IS), the Innovative Practice Bases of Geological Engineering and Surveying Engineering of Southwest Jiaotong University (YJG-2022-JD04).

Author contributions Xie Zhuowu: Conceptualization, Writing Original draft, investigation, experiments, data organization. Liao Xin: Data analysis, revision. Inna Safonova: Supervision, Validation, Writing – review & editing. Wei Wei: Editing. Sixiang Ling: Assist in experiments. Sergei Krivonogov: Writing - review & editing. Wu Xiyong: Funding acquisition.

Declarations

Competing interests The authors declare that they have no known competing financial interests or personal relationships that could have appeared to influence the work reported in this paper.

References

Barshad I (1952) Absorptive and swelling properties of clay-water system. Clay Clay Min 1:70–77. https://doi.org/10.1038/155154a0

Bond JJ, Willis WO (1969) Soil water evaporation: surface residue rate and placement effects. Soil Sci Soc Am J 33(3):445–448. https://doi.org/10.2136/sssaj1969.03615995003300030031x

Bureau SG (1980) Regional Geological Survey Report (Suining, Zigong, Neijiang, Yibin and Luzhou Geological Map Sheet, 1: 200000), Chengdu: Sichuan Geology Bureau. https://doi.org/10.17077/2160-5270.1305

Chen YL, Ni J, Shao W, Azzam R (2012) Experimental study on the influence of temperature on the mechanical properties of granite under uni-axial compression and fatigue loading. Int J Rock Mech Min Sci 56:62–66. https://doi.org/10.1016/j.ijrmms.2012.07.026

Cliff TJ (2018) 4 - Clay mineral–water interactions. Developments Clay Sci 9:89–124. https://doi.org/10.1016/B978-0-08-102432-4.00004-4

Dai Z, Guo J, Yu F, Zhou Z, Li J, Chen S (2021) Long-term uplift of high-speed railway subgrade caused by swelling effect of red-bed mudstone: case study in Southwest China. B Eng Geol Environ 80:4855–4869. https://doi.org/10.1007/s10064-021-02220-7

Delage P, Marcial D, Cui YJ, Ruiz X (2006) Ageing effects in the compacted bentonite: a microstructure approach. Géotechnique 56(4):291–304. https://doi.10.1680/geot.2006.56.5.291

Doostmohammadi R, Moosavi M, Mutschler T, Osan C (2009) Influence of Cyclic wetting and drying on swelling behavior of mudstone in South West of Iran. Environ Geol 58:999–1009. https://doi.org/10.1007/s00254-008-1579-3

Fernandes J, Fernandes AC, Echeverría JC, Moriones P, Garrido JJ, Pires J (2019) Adsorption of gases and vapours in silica based xerogels. Colloid Surf A 561:128–135. https://doi.org/10.1016/j.colsurfa.2018.10.063

Ferrero AM, Marini P (2001) Experimental studies on the mechanical behaviour of two thermal cracked marbles. Rock Mech Rock Eng 34 (1): 57–66. https://doi.10.1007/s006030170026

Gautam PK, Verma AK, Jha MK, Sharma P, Singh TN (2018) Effect of high temperature on physical and mechanical properties of Jalore granite. J Appl Geophys 159:460–474. https://doi.org/10.1016/j.jappgeo.2018.07.018

Huang K, Yu F, Zhang W, Tong K, Guo J, Li S, Chen S, Dai Z (2023) Relationship between capillary water absorption mechanism and pore structure and microfracture of red-layer mudstone in central Sichuan. Bull Eng Geol Environ 82:100. https://doi.org/10.1007/s10064-023-03115-5

Hueckel T (1992) On effective stress concepts and strain in clays subjected to environmental loads: discussion. Can Geotech J 29:1120–1125. https://doi.org/10.1139/t92-130

Jin PH, Hu YQ, Shao JX, Liu ZJ, Feng G, Song S (2020) Influence of temperature on the structure of Pore–Fracture of sandstone. Rock Mech Rock Eng 53:1–12. https://doi.org/10.1007/s00603-019-01858-w

Karaborni S, Smit B, Heidug W, Urai J, van Oort E (1996) The swelling of clays: molecular simulations of the hydration of montmorillonite. Science 271(5252):1102–1104. https://doi.org/10.1126/science.271.5252.1102

Kumari WGP, Ranjith PG, Perera MSA, Chen BK, Abdulagatov IM (2017) Temperature-dependent mechanical behaviour of Australian Strathbogie granite with different cooling treatments. Eng Geol 229:31–44. https://doi.org/10.1016/j.enggeo.2017.09.012

Lahn L, Bertier P, Seemann T, Stanjek H (2019) Distribution of sorbed water in the pore network of mudstones assessed from physisorption measurements. Micropor Mesopor Mat 295:109902. https://doi.org/10.1016/j.micromeso.2019.109902

Laird DA (2006) Influence of layer charge on swelling of smectites. Appl Clay Sci 34(1):74–87. https://doi.org/10.1016/j.clay.2006.01.009

Li J, Wang S, Lu S, Zhang P, Cai J, Zhao J, Li W (2019) Microdistribution and mobility of water in gas shale: A theoretical and experimental study. Mar Petrol Geol 102:496–507. https://doi.org/10.1016/j.marpetgeo.2019.01.012

Li P, Zhang J, Rezaee R, Dang W, Tang X, Nie H, Chen S (2021) Effect of adsorbed moisture on the pore size distribution of marine-continental transitional shales: insights from lithofacies differences and clay swelling. Appl Clay Sci 201:105926. https://doi.org/10.1016/j.clay.2020.105926

Liu S, Xu J (2014) Mechanical properties of Qin Ling biotite granite after high temperature treatment. Int J Rock Mech Min Sci 71:188–193. https://doi.org/10.1016/j.ijrmms.2014.07.008

Liu Y, Ji P, Fang L (1999) Approach to Cyclic swelling behavior of compacted expansive clays. Chin J Geotech Eng Chin J Geotech Eng. (01),12–16

Liu CD, Cheng Y, Jiao YY, Zhang GH, Zhang WS, Ou GZ, Tan F (2021a) Experimental study on the effect of water on mechanical properties of swelling mudstone. Eng Geol 295:106448. https://doi.org/10.1016/j.rineng.2022.100728

Liu LB, Zhang C, Jiang WJ, Li X, Dai YC, Jia HZ (2021b) Understanding the sorption behaviors of heavy metal ions in the interlayer and nanopore of montmorillonite: a molecular dynamics study. J Hazard Mater 416, 125976. https://doi.10.1016/j.jhazmat.2021.125976

Lu X, Zhou W, Cai Q, Li M, Luan B, Liu F (2021) Mechanical properties and meso fracture mechanism of mudstone under freeze-thaw cycle. J Min Saf Eng 38(4):819. https://doi.org/10.1051/e3sconf/201913604048

Miller AK, Guggenheim S, van Groos AFK (1991) Bond energy of adsorbed and interlayer water: kerolite dehydration at elevated pressures. Clay Clay Min 39:127–130. https://doi.org/10.1346/CCMN.1991.0390202

Mitchell JK (1993) Fundamentals of soil behavior, 2nd edn Wiley New York. https://doi.10.1016/0167-5699(84)90157-9

Okamoto R, Sugahara H, Hirano I (1981) Slaking and swelling properties of mudstone. In ISRM International Symposium (pp. ISRM-IS) ISRM

Pejon OJ, Zuquette LV (2002) Analysis of Cyclic swelling of mudrocks. Eng Geol 67(1–2):97–108. https://doi.org/10.1016/S0013-7952(02)00147-3

PRC National Standard (2013) GB/T 50266–2013 standard for test methods of engineering rock mess China standards press Beijing (in Chinese). https://doi.org/10.1201/b14917-8

Pusch R, Karlnland O, Hokmark H (1990) GMM-a general microstructural model for qualitative and quantitative studies of smectite clays. SKB Tech Rep TR-90-43 SKB Stockholm Swed. https://doi.org/10.1162/qss_e_00061

Saiyouri N, Hicher PY, Tessier D (2000) Microstructural approach and transfer water modelling in highly compacted unsaturated swelling clays. Mech Cohesive Frict Mater 5(1):41–60. https://doi.org/10.1002/(SICI)1099-1484(200001)5:1-41::AID-CFM75-3.0.CO;2-N

Shen YJ, Li ZY, Peng C, Yang BH, Ma TC (2023) Experimental studies on the effects of thermal damage in coal-derived mudstones caused by high temperatures. Acta Geod Geoph 58:649–667. https://doi.org/10.1007/s40328-023-00431-w

Singh B, Ranjith PG, Chandrasekharam D, Viete D, Singh HK, Lashin A, Al Arifi N (2015) Thermo-mechanical properties of Bundelkhand granite near Jhansi, India. Geomechan Geoph Geo-Energy Geo-Resources 1:35–53. https://doi.org/10.1007/s40948-015-0005-z

Sirdesai NN, Singh TN, Ranjith PG, Singh R (2017) Effect of varied durations of thermal treatment on the tensile strength of red sandstone. Rock Mech Rock Eng 50:205–213. https://doi.org/10.1007/s00603-016-1047-4

Sirdesai NN, Gupta T, Singh TN, Ranjith PG (2018) Studying the acoustic emission response of an Indian monumental sandstone under varying temperatures and strains. Constr Build Mater 168:346–361. https://doi.org/10.1016/j.conbuildmat.2018.02.180

Taylor RK, Smith TJ (1986) The engineering geology of clay minerals: swelling, shrinking and mudrock breakdown. Clay Min 21(3):235–260. https://doi.org/10.1180/claymin.1986.021.3.01

Thommes M, Kaneko K, Neimark AV, Olivier JP, Rodriguez-Reinoso F, Rouquerol J, Sing KSW (2015) Physisorption of gases, with special reference to the evaluation of surface area and pore size distribution (IUPAC Technical Report). Pure and Applied Chemistry 87(9–10). https://doi.org/10.1515/pac-2014-1117

Tian H, Kempka T, Xu NX, Ziegler M (2012) Physical properties of sandstones after high temperature treatment. Rock Mech Rock Eng 45:1113–1117. https://doi.org/10.1007/s00603-012-0228-z

Tian H, Ziegler M, Kempka T (2014) Physical and mechanical behavior of claystone exposed to temperatures up to 1000°C. Int J Rock Mech Min 70:144–153. https://doi.org/10.1016/j.ijrmms.2014.04.014

Towhata I, Kuntiwattanaku P, Seko I, Ohishi K (1993) Volume change of clays induced by heating as observed in consolidation tests. Soils Found 33(4):170–183. https://doi.org/10.3208/sandf1972.33.4_170

Van Geet M, Volckaert G, Roels S (2005) The use of microfocus X-ray computed tomography in characterising the hydration of a clay pellet/powder mixture. Appl Clay Sci 29(2):73–87. https://doi.org/10.1016/j.clay.2004.12.007

Wong LNY, Zhang Y, Wu Z (2020) Rock strengthening or weakening upon heating in the mild temperature range. Eng Geol 272:105619. https://doi.org/10.1016/j.enggeo.2020.105619

Wu P, Ming C (2006) The relationship between acidic activation and microstructural changes in montmorillonite from Heping China. Spectrochimica Acta Part A: Molecular and Biomolecular Spectroscopy 63(1): 85–90. https://doi.10.1016/j.saa.2005.04.050

Xu XL, Gao F, Shen XM, Jin CH (2010) Research on mechanical characteristics and micropore structure of granite under high-temperature. Rock Soil Mech 06:1752–1758. https://doi.org/10.16285/j.rsm.2010.06.039

Yang SQ, Ranjith PG, Jing HW, Tian WL, Ju Y (2017a) An experimental investigation on thermal damage and failure mechanical behavior of granite after exposure to different high temperature treatments. Geothermics 65:180–197. https://doi.org/10.1016/j.geothermics.2016.09.008

Yang SQ, Xu P, Li YB, Huang YH (2017b) Experimental investigation on triaxial mechanical and permeability behavior of sandstone after exposure to different high temperature treatments. Geothermics 69:93–109. https://doi.org/10.1016/j.geothermics.2017.04.009

Yavuz H, Demirdag S, Caran S (2010) Thermal effect on the physical properties of carbonate rocks. Int J Rock Mech Min Sci 47(1):94–103. https://doi.org/10.1016/j.ijrmms.2009.09.014

Yin T, Wang P, Li X, Wu B, Tao M, Shu R (2016) Determination of dynamic flexural tensile strength of thermally treated Laurentian granite using semi-circular specimens. Rock Mech Rock Eng 49:3887–3898. https://doi.org/10.1007/s00603-016-0920-5

Zhang CL, Wieczorek K, Xie ML (2010) Swelling experiments on mudstones. J Rock Mechan Geotech Eng 2(1):44–51. https://doi.org/10.1016/j.jrmge.2022.07.014

Zhang W, Sun Q, Hao S, Geng J, Lv C (2016a) Experimental study on the variation of physical and mechanical properties of rock after high temperature treatment. Appl Therm Eng 98:1297–1304. https://doi.org/10.1016/j.applthermaleng.2016.01.010

Zhang ZZ, Gao F, Gao Y, Xu XL, Hou P, Teng T, Shang XJ (2016b) Fractal structure and model of pore size distribution of granite under high temperatures. Chin J Rock Mech Eng 35:2426–2438. https://doi.org/10.13722/j.cnki.jrme.2016.0798

Zhang WQ, Sun Q, Zhu SY, Wang B (2017) Experimental study on mechanical and porous characteristics of limestone affected by high temperature. Appl Therm Eng 110:356–362. https://doi.org/10.1016/j.applthermaleng.2016.08.194

Zhang WL, Mo F, Qi ZL, Huang XL, Yue P, Liu QS, Wan Q, Fu WT (2024) Imbibition mechanism of water in illite nanopores of deep shales by molecular simulation. J Mol Liq 126232. https://doi.org/10.1016/j.molliq.2024.126232